

Supporting Information

Aqueous organic redox-targeting flow battery based on
Nernstian-potential-driven anodic redox-targeting reaction

Hongchao Zhang,^{†a} Qinghong Huang,^{†b} Xue Xia,^a Yanjun Shi,^a Yong-Miao Shen,^c
Juan Xu,^{a*} Zhidong Chen and Jianyu Cao^{a*}

^a*Jiangsu Key Laboratory of Advanced Catalytic Materials and Technology,
Changzhou University, Changzhou 213164, China.*

^b*State Key Laboratory of Materials-Oriented Chemical Engineering, College of
Energy Science and Engineering, Nanjing Tech University, Nanjing 211816, China*

^c*Department of Chemistry, Zhejiang Sci-Tech University, Hangzhou 310018, China.*

[†]H. Z. and Q. H. contributed equally.

*Corresponding author. E-mail: jycao@cczu.edu.cn (Jianyu Cao);
cjytion@cczu.edu.cn (Juan Xu)

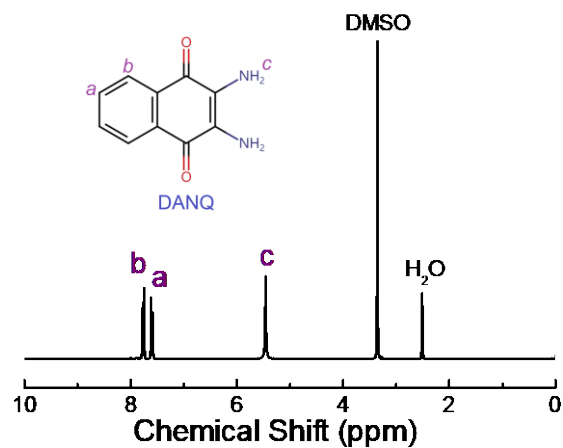


Fig. S1 ¹H NMR spectrum of DANQ (400 MHz, DMSO-d₆). δ (ppm) 5.46 (s, 4H, -NH₂), 7.59 (m, 2H), 7.76 (m, 2H).

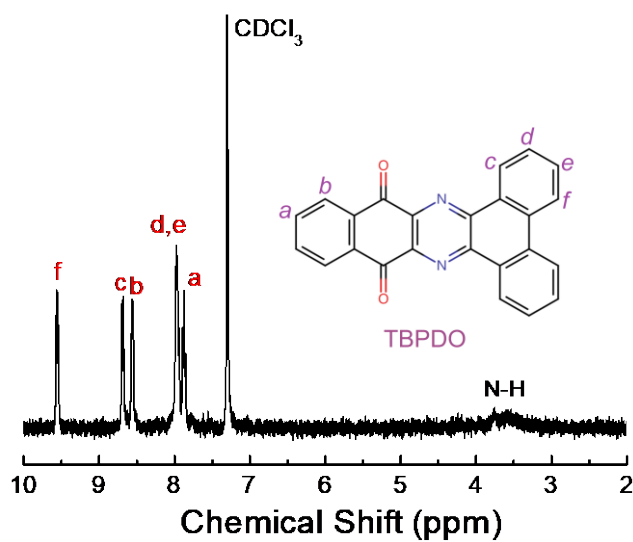


Fig. S2 ¹H NMR spectrum of TBPDO (400 MHz, CDCl₃). δ (ppm) 7.86-7.89 (t, 2H), 7.94-7.98 (m, 4H), 8.55-8.57 (t, 2H), 8.68-8.70 (d, 2H), 9.54-9.56 (d, 2H).

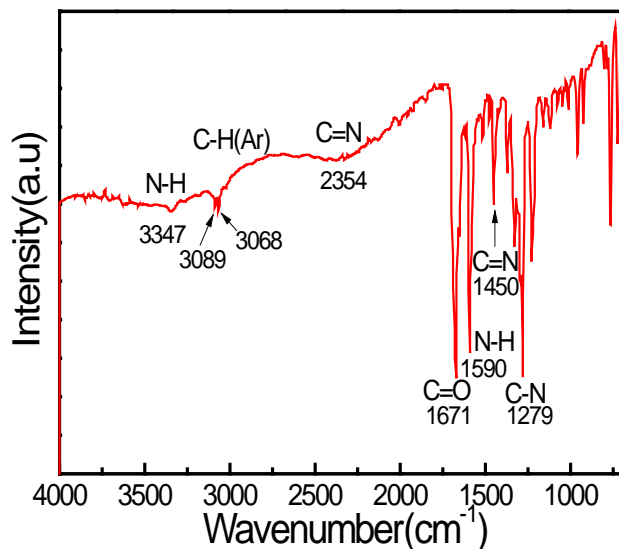


Fig. S3 FT-IR spectrum of TBPDO. FT-IR (cm^{-1}) 3347 (N-H), 3089/3068 (C-H, Ar), 2354(C=N), 1671(C=O), 1590(N-H), 1450(C=N) and 1279(C-N).

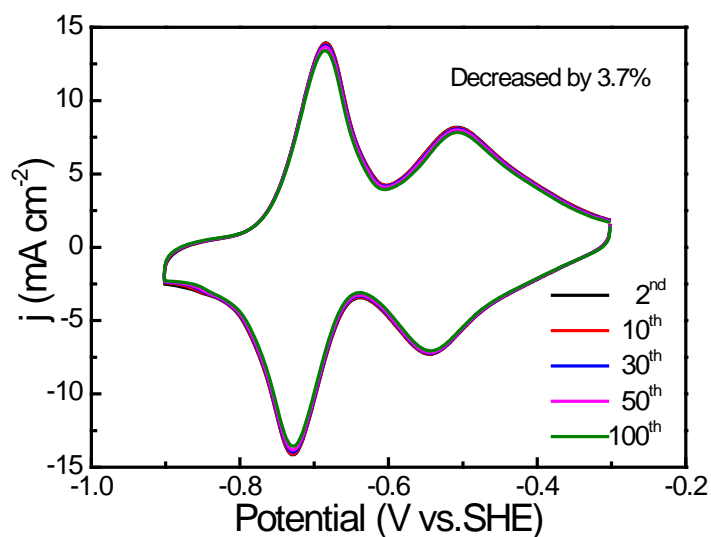


Fig. S4 CVs of TBPDO electrode with acidified KB as the conductive additive in a 1 M KOH solution at 100 mV s^{-1} during the 2nd, 10th, 30th, 50th and 100th cycles.

Determination of diffusion coefficient and charge transfer rate constant

Fig. S5 shows CVs of TBPDO electrode in 1 M KOH solution at different scan rates. The applied scan rate ranges from 0.005 to 4 V s^{-1} . When the scan rate is higher

than 0.4 V s^{-1} , the peak currents for both ET1 and ET2 are linearly increased with the increase of the square root of the scan rates (**Fig. S6a-S6b**), revealing the characteristic of diffusion-controlled process at high scan rates for TBPDO electrode. The chronoamperometry curves (**Fig. S7a-S7b**) were recorded and fitted to determine the diffusion coefficients for ET1 and ET2 of TBPDO electrode using the following semi-infinite linear diffusion Cottrell equation [S1]:

$$j = nFC_s\left(\frac{D}{\pi t}\right)^{1/2} \quad (2)$$

where D is the diffusion coefficient, j is the current density, t is time, n is the number of transferred electrons, F is the Faraday constant and C_s is the concentration of redox species within the TBPDO electrode layer.

The concentration (C_s) of redox species is calculated by the equation [S2] as follow:

$$C_s = \frac{m}{M_w A \delta} \quad (3)$$

where m is the mass of TBPDO ($5.58 \mu\text{g}$), M_w is the molecular weight of TBPDO (360 g mol^{-1}), A is the geometric area of electrode (0.071 cm^2) and δ is the average thickness of TBPDO electrode layer that was obtained using a Dektak step profiler ($3.57 \mu\text{m}$, **Table S1**). Therefore, the C_s value was calculated to be 0.603 mol L^{-1} .

The Cottrell plots of both ET1 and ET2 reveal good linear dependence of j versus $t^{-1/2}$. According to the linear dependence of j versus $t^{-1/2}$ for the Cottrell plots (**Fig. S7c-S7f**), the D values of the oxidation and reduction progress for ET1 are calculated to be 1.59×10^{-12} and $3.07 \times 10^{-12} \text{ cm}^2 \text{ s}^{-1}$ while the D values of the oxidation

and reduction progress for ET2 are 6.67×10^{-13} and $7.28 \times 10^{-13} \text{ cm}^2 \text{ s}^{-1}$, respectively. Therefore, the average D values for ET1 and ET2 are determined to be 2.33×10^{-12} and $6.97 \times 10^{-13} \text{ cm}^2 \text{ s}^{-1}$, respectively.

The charge transfer rate constant (k^0) is obtained by using Nicholson's method [S3]. Firstly, the kinetic parameter Ψ was obtained from the potential gap between the oxidation and reduction peak (ΔE_p) using the following equation:

$$\Psi = (-0.6288 + 0.0021\Delta E_p)/(-0.017\Delta E_p + 1) \quad (4)$$

Then, k^0 was calculated according to the linear relationship between Ψ and $\nu^{-1/2}$ shown in the equation (5).

$$\Psi = k^0 \left(\frac{\pi D n F}{RT} \right)^{-1/2} \nu^{-1/2} \quad (5)$$

Therefore, the k^0 values were calculated to be $8.21 \times 10^{-4} \text{ cm s}^{-1}$ for ET1 and $1.59 \times 10^{-3} \text{ cm s}^{-1}$ for ET2, respectively, from the slope of the $\Psi \sim \nu^{-1/2}$ dependence (Fig. S8a-S8b).

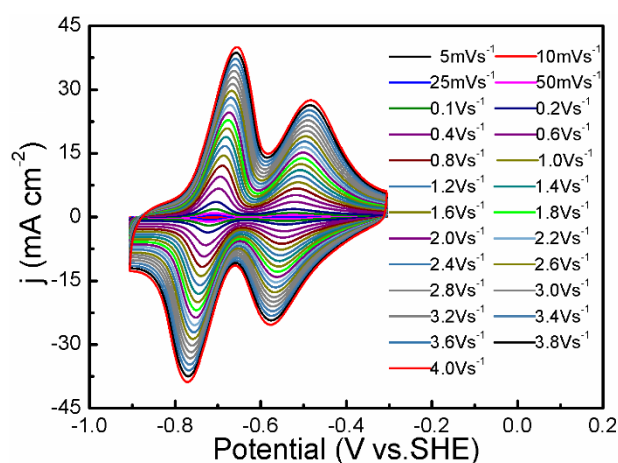


Fig. S5 CVs of TBPDO electrode in 1 M KOH solution at different scan rates (the scan rates (ν) from 0.005 to 4 V s⁻¹).

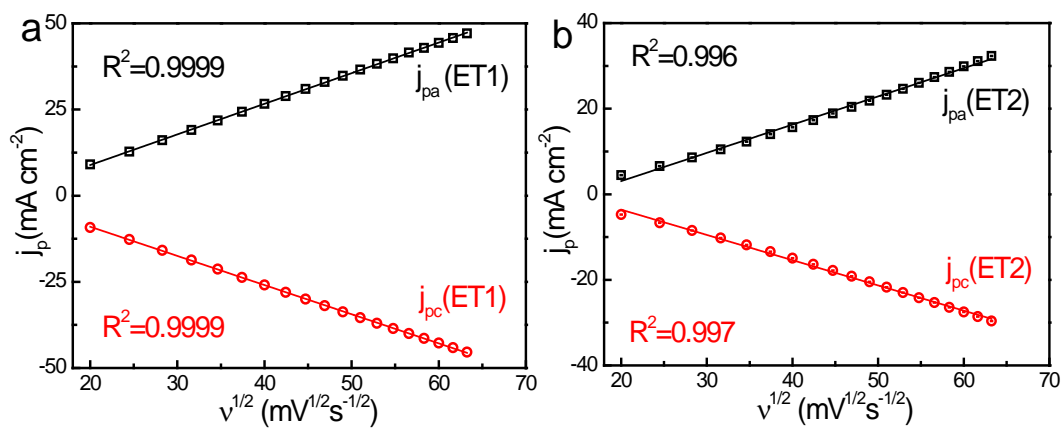


Fig. S6 Plots of peak current density (j_p) versus square root of scan rate ($v^{1/2}$) for ET1 (a) and ET2 (b), respectively.

Table S1 Thickness data of the TBPDO electrode layer obtained from Dektak step profiler (Bruker).

| No. | 1 | 2 | 3 | 4 | Average value |
|-----------------------------|------|------|------|------|---------------|
| Thickness (μm) | 3.78 | 3.36 | 3.35 | 3.78 | 3.57 |

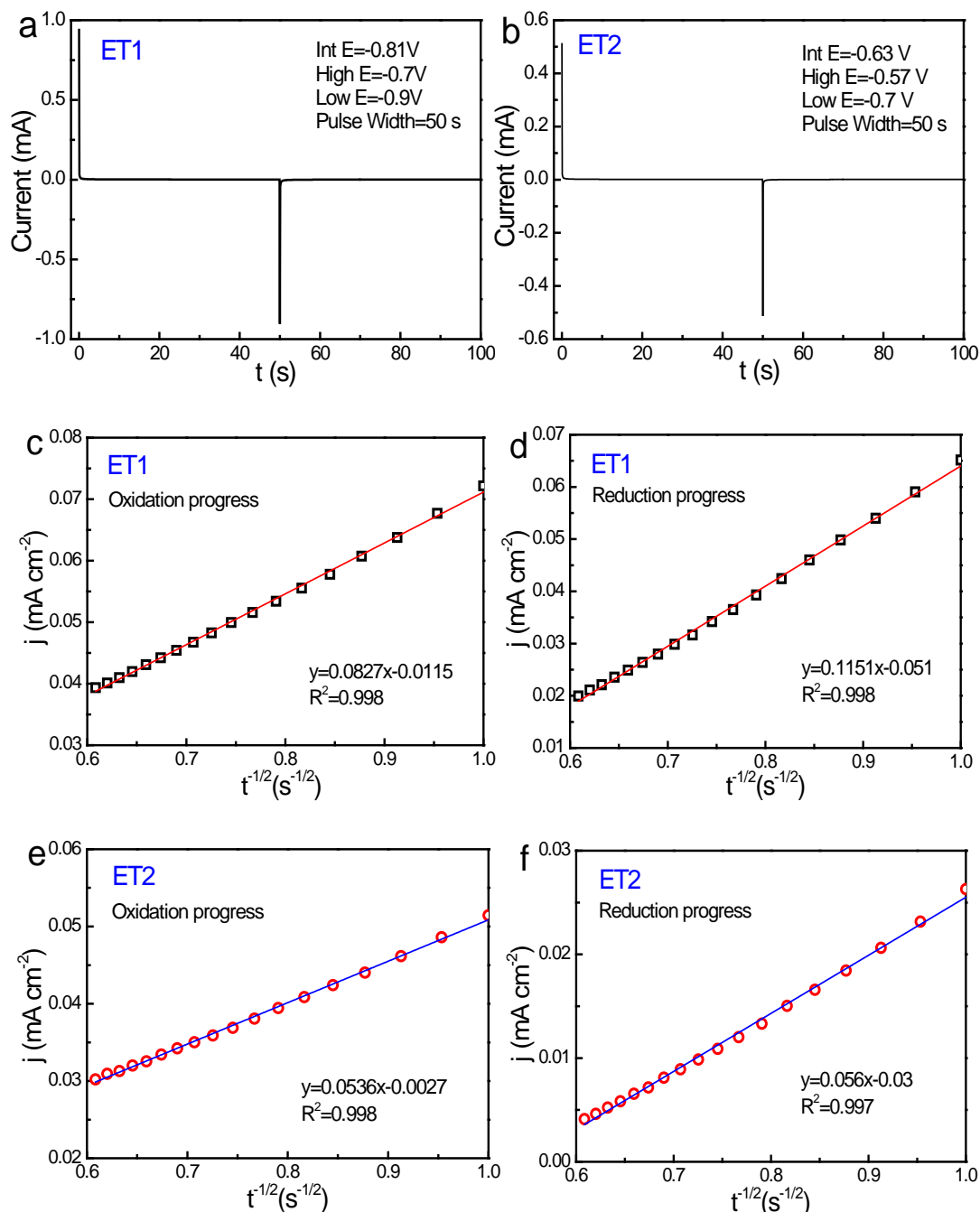


Fig. S7 The chronoamperometry curve of TBPDO electrode in 1 M KOH solution for (a) ET1 and (b) ET2. (c) Cottrell plot of ET1 for the oxidation reaction. (d) Cottrell plot of ET1 for the reduction reaction. (e) Cottrell plot of ET2 for the oxidation reaction. (f) Cottrell plot of ET2 for the reduction reaction. The results of the linear regression are also shown.

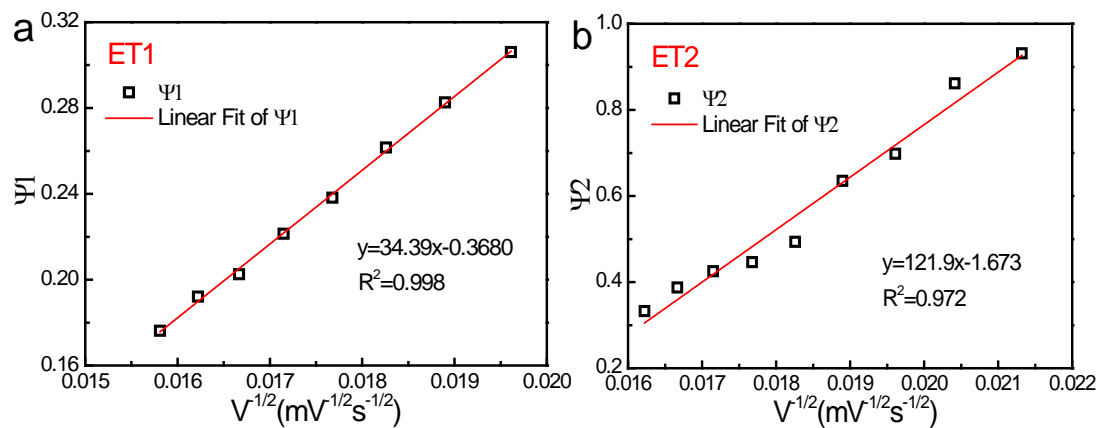


Fig. S8 (a) Plot of Ψ versus $v^{-1/2}$ for ET1 (The linear relationship was shown with scan rates of 2.6~4.0 V s^{-1}). (b) Plot of Ψ versus $v^{-1/2}$ for ET2 (The linear relationship was shown with scan rates of 2.2~3.8 V s^{-1}).

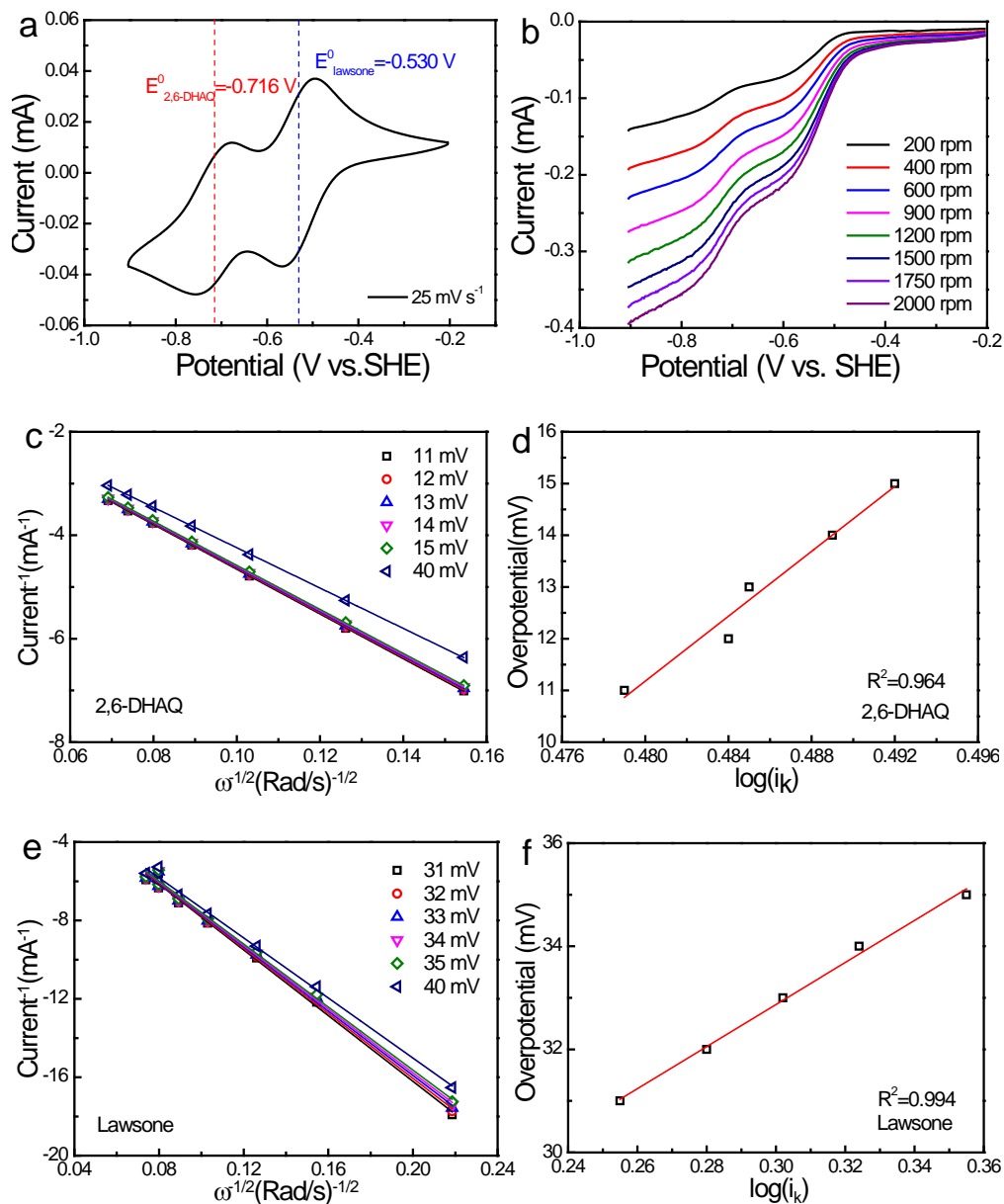


Fig. S9 (a) CV curve of 1 mM anthrafravic acid + 1 mM lawsone in 1 M KOH at 25 mV s^{-1} . (b) RDE voltammetry curves of 1 mM anthrafravic acid + 1 mM lawsone in 1 M KOH at eight rotation rates ranging from 200 to 2000 rpm. (c, e) Koutecky-Levich plots derived from these RDE data at different oxidation overpotentials. (d, f) Fitted curves of Butler-Volmer equation using the kinetic current density (j_k) obtained from the zero-intercept of Koutecky-Levich plots in (c, e) at five oxidation overpotentials.

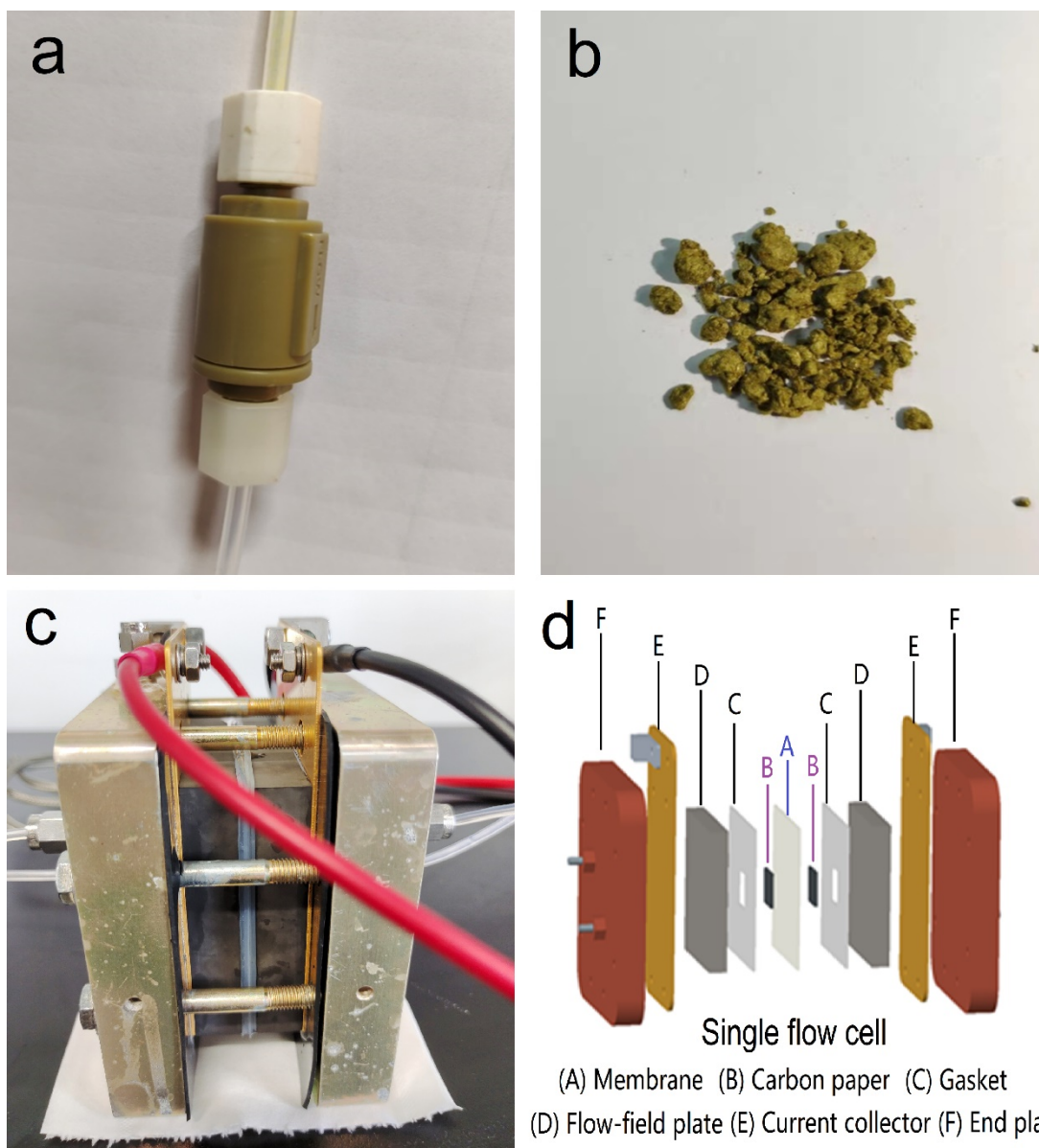


Fig. S10 Digital photos of the container and granules. (a) The container of the solid-state energy storage material. (b) granules of TBPDO. (c) the flow cell with an active area of 5 cm^2 . (d) the exploded view of the flow cell.

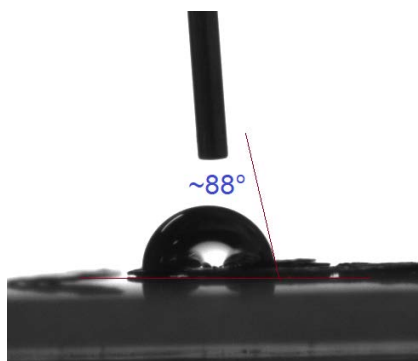


Fig. S11 The contact angle of water on the compacted TBPDO powder surface.

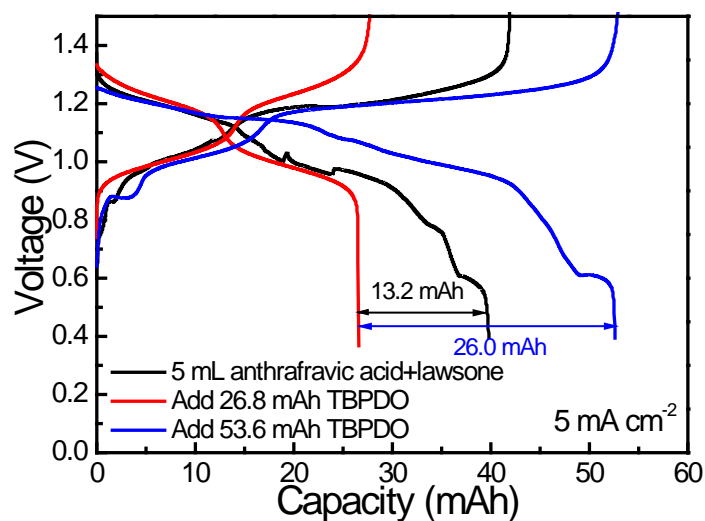


Fig. S12 Voltage profiles of the RTFB cell with 26.8 and 53.6 mAh TBPDO, respectively, at 5 mA cm^{-2} . 5 mL 50 mM anthrafravic acid + 50 mM lawsone in 1 M KOH was utilized as an anolyte. 10 mL 300 mM $\text{K}_4[\text{Fe}(\text{CN})_6]$ + 75 mM $\text{K}_3[\text{Fe}(\text{CN})_6]$ in 1 M KOH was used as a catholyte for the cell with 26.8 mAh TBPDO while 20 mL 300 mM $\text{K}_4[\text{Fe}(\text{CN})_6]$ + 75 mM $\text{K}_3[\text{Fe}(\text{CN})_6]$ in 1 M KOH was used as a catholyte for the cell with 53.6 mAh TBPDO.

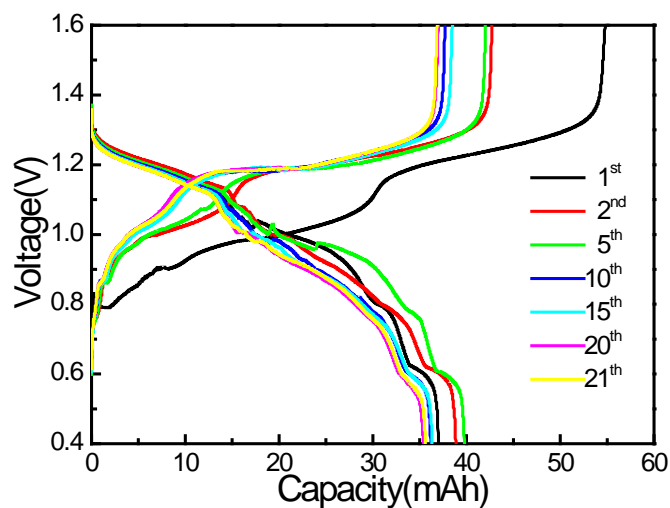


Fig. S13 Representative charge-discharge profiles of 5 mL 50 mM anthrafravic acid + 50 mM lawsone//ferrocyanide flow cell after adding 26.8 mAh (90 mg) TBPDO at 5 mA cm⁻².

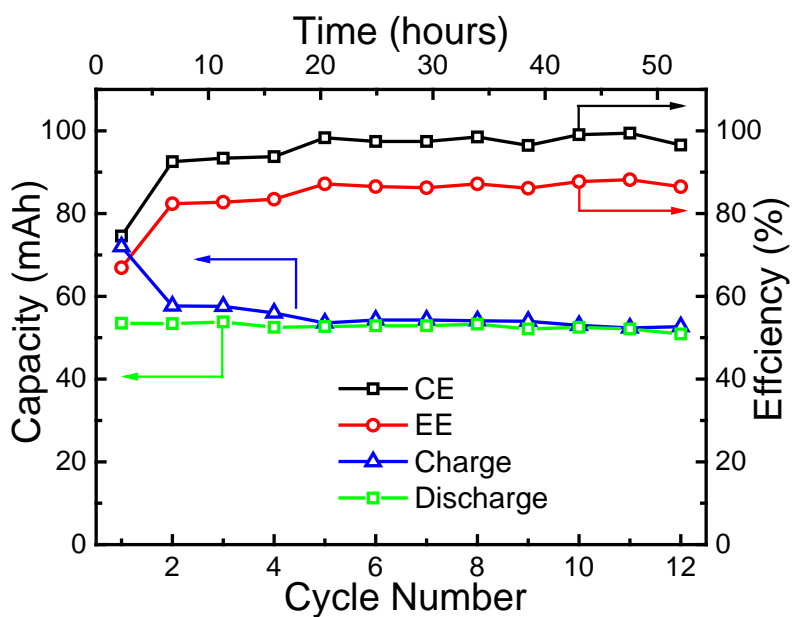


Fig. S14 Capacity retention and efficiencies of the RTFB cell after adding 53.6 mAh (180 mg) TBPDO at a constant current density of 5 mA cm⁻².

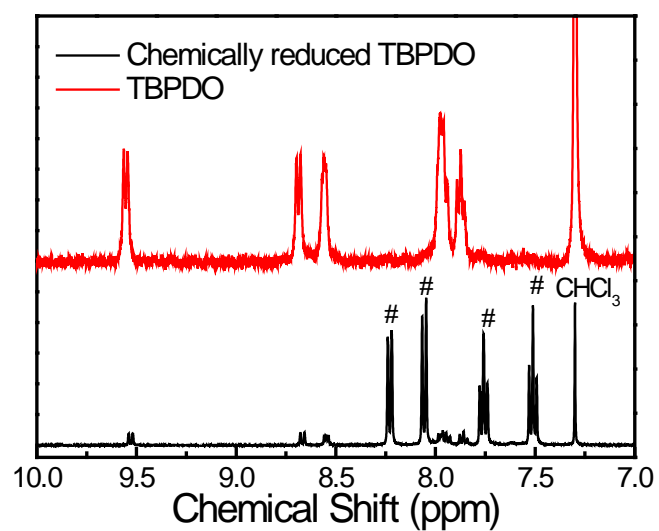


Fig. S15 ¹H NMR spectra of pristine and chemically reduced TBPDO by NaBH₄ in CDCl₃.

Table S2 Comparison of performances of anodic energy-storage materials for aqueous RTFBs. ESM, energy-storage material; ML, mass loading of ESM; C_{theo} , theoretical capacity of ESM; MUR, material utilization rate; SC, specific capacity based on the volume of the anolyte; CE, current efficiency; EE, energy efficiency; CRPC, capacity retention per cycle; TCFR, temporal capacity fade rate. PANI, polyaniline; CB, carbon black. NA, not applicable.

| ESM | ML (mg) | C_{theo} (mAh g ⁻¹) | MUR | SC (AhL ⁻¹) | CE | EE | CRPC | TCFR |
|--|-----------------------------------|---|---|---|-----------------------------------|-----------------------------------|----------------------------------|------------------|
| PANI/CB ^[S4] | 7400 | 144 | 44.1% at 15.4 mA cm ⁻² | 35.8 at 15.4 mA cm ⁻² | NA | NA | ~98.8% per cycle (10 cycles) | ~2% per day |
| Polyimide/CB ^[S5] | 360 (54 mAh) &780 (117 mAh) | 150 | 83% at 10 mA cm ⁻² & 61% at 30 mA cm ⁻² | ~22 at 30 mA cm ⁻² | ~98% at 30 mA cm ⁻² | NA | ~99.9% per cycle (~60 cycles) | ~1% per day |
| LiTi ₂ (PO ₄) ₃ /C ^[S6] | ~670 | 138 | 14% at 2.5 mA cm ⁻² | ~6.9 at at 2.5 mA cm ⁻² | ~98% at 5 mA cm ^{-2*} | ~70% at 5 mA cm ^{-2*} | 99.98% (~55 cycles)* | NA |
| TBPDO (this work) | 90 (26.8 mAh) & 180 (53.6 mAh) | 298 | 80.2% at 2 mA cm ⁻² | 8.3 at 2 mA cm ⁻² & 10.3 at 5 mA cm ⁻² | ~95% at 5 mA cm ⁻² | ~81% at 5 mA cm ⁻² | 99.82% per cycle (21 cycles) | 1.44% per day |

* The anode is not the capacity limiting side.

References

- [S1] A. J. Bard, L. R. Faulkner, Fundamentals and applications. Electrochemical methods **2001**, 2, 482; K. Sato, R. Ichinoi, R. Mizukami, T. Serikawa, Y. Sasaki, J. Lutkenhaus, H. Nishide, K. Oyaizu, *J. Am. Chem. Soc.* **2018**, *140*, 1049.
- [S2] Y. Zhang, J. Cao, Z. Chen, J. Xu, C. Yu, *J. Mater. Chem. A*, **2020**, *8*, 6874.
- [S3] J. Luo, A. Sam, B. Hu, C. DeBruler, X. Wei, W. Wang, T. L. Liu, *Nano Energy* **2017**, *42*, 215.
- [S4] E. Zanzola, C.R. Dennison, A. Battistel, P. Peljo, H. Vrubel, V. Amstutz, H. H. Girault, *Electrochim. Acta* **2017**, *235*, 664-671.
- [S5] M. Zhou, Y. Chen, M. Salla, H. Zhang, X. Wang, S. R. Mothe and Q. Wang, *Angew. Chem. Int. Ed.* 2020, **59**, 1-7.
- [S6] J. Yu, L. Fan, R. Yan, M. Zhou, Q. Wang, *ACS Energy Lett.* 2018, **3**, 2314-2320.